Available online at www.sciencedirect.com
SCIENCE DIRECT®
Journal of Computational Physics 198 (2004) 659–685
JOURNAL OF COMPUTATIONAL PHYSICS
www.elsevier.com/locate/jcp

The pressure-corrected ICE finite element method for compressible flows on unstructured meshes

Richard C. Martineau *, Ray A. Berry

Idaho National Engineering and Environmental Laboratory, P.O. Box 1625, Idaho Falls, ID 83415, USA

Received 3 September 2003; received in revised form 17 January 2004; accepted 26 January 2004
Available online 17 March 2004

Abstract

A new implicit continuous-fluid Eulerian (ICE) scheme for simulating a wide range of transient and steady, inviscid and viscous compressible flows on unstructured finite elements is presented. This new computational fluid dynamics scheme, termed the pressure-corrected ICE-finite element method (PCICE-FEM), represents an advancement in mass–momentum coupled, pressure-based schemes. The governing hydrodynamic equations for this scheme consist of the conservative forms of the momentum balance (Navier–Stokes), mass conservation, and total energy equations. The PCICE-FEM scheme is developed as a predictor–corrector scheme by performing a fractional-step splitting of the semi-implicit temporal discretization of the governing equations into an explicit predictor phase and a semi-implicit pressure-correction phase coupled by a pressure Poisson solution. The result of this predictor–corrector formulation is that the pressure Poisson equation is provided with sufficient internal energy information to avoid iteration with the semi-implicit pressure-correction equations. The PCICE-FEM scheme combines a modified form of the two-step Taylor–Galerkin FEM scheme as an explicit predictor for the fractional momentum equations and a time-weighted FEM method for the semi-implicit form of the mass conservation and the total energy equations. The PCICE-FEM scheme employs flux-corrected transport (FCT) as a high-resolution filter for shock capturing. The ability of the PCICE-FEM scheme to accurately and efficiently simulate a wide variety of flows from nearly incompressible to highly compressible is demonstrated.

Keywords: ICE; Fractional-step; Predictor–corrector; Pressure Poisson equation; FEM; Flux-corrected transport

1. Introduction

Generally, semi-implicit pressure-based schemes for compressible flow require an iterative process to satisfy conservation of mass and energy requirements. Most pressure-based schemes first solve the pressure Poisson equation with information from an explicit (predicted) momentum balance solution. A correction

* Corresponding author. Tel.: +1-208-526-2938; fax: +1-208-526-0875.
E-mail address: rcm@inel.gov (R.C. Martineau).

0021-9991/$ - see front matter © 2004 Elsevier Inc. All rights reserved.
doi:10.1016/j.jcp.2004.01.034

of mass and momentum is then determined with the new pressure field obtained from the pressure Poisson solution. The energy equation is then explicitly advanced in time with the new mass, momentum, and pressure. However, the new energy solution is generally not consistent with mass, momentum, and pressure because information from the new energy solution was required for full coupling of the energy equation with the pressure Poisson equation. Therefore, the updated (corrected) values of mass, momentum, and energy are then used to re-solve the pressure Poisson equation. A new pressure field is computed, from which, a new set of pressure corrected conserved variables are then determined. This iterative process continues until simultaneous convergence on pressure, mass, and energy is achieved.

We present a new computational fluid dynamics (CFD) scheme developed for compressible flows that improves upon previous pressure-based methods in terms of accuracy and numerical efficiency with a wider range of applicability. Based on the implicit continuous-fluid Eulerian (ICE) scheme originally developed by Harlow and Amsden [1,2], a new algorithm, termed the pressure-corrected implicit continuous-fluid Eulerian (PCICE), is combined with the finite element method (FEM) spatial discretization scheme to yield a new semi-implicit pressure-based scheme for compressible flows named the PCICE-FEM scheme [3]. In the PCICE algorithm, the total energy equation is sufficiently coupled to the pressure Poisson equation through the equation of state to avoid iteration between the pressure Poisson equation and the pressure-correction equations. Both the mass conservation and total energy equations are explicitly convected with the time-advanced explicit momentum solution to provide the pressure Poisson equation with the time-advanced internal energy information it requires. At the end of a time step, the conserved values of mass, momentum, and total energy are all pressure-corrected. As a result, the iterative process discussed above is not required. This aspect is advantageous when computing transient flows that are highly compressible and/or contain significant energy deposition.

The PCICE algorithm is composed of three phases: an explicit predictor, an elliptic pressure Poisson solution, and a semi-implicit pressure-correction of the flow variables. The pressure, momentum, and density variables in the governing hydrodynamic equations are treated implicitly. Hence, the formulation is referred to as *semi-implicit*. The three implicit variables are directly coupled by substituting the momentum balance equations into the mass conservation equation to eliminate momentum (or mass flux) as an unknown. This substitution is known as *mass–momentum coupling*. The time rate of density change in the mass conservation equation is then expressed in terms of pressure and energy by employing the equation of state. These substitutions result in a single second-order elliptic differential equation in terms of pressure (pressure Poisson equation). Thus, the scheme is termed *pressure-based*. The solution of the pressure Poisson equation effectively solves the mass conservation and momentum balance equations simultaneously. This semi-implicit treatment has two advantages over explicit schemes. First, the acoustic component from the explicit time step size stability criteria is removed. This eliminates the time integration stiffness that results from slow flows in small computational cells, such as those found in viscous boundary layer discretizations. The second advantage is that the pressure obtained with this semi-implicit treatment corrects the momentum to satisfy mass conservation requirements. This, in theory, allows incompressible flows to be simulated with compressible flow equations. This type of scheme can then be used to simulate any flow from nearly incompressible to supersonic.

The PCICE-FEM scheme incorporates a combination of the two-step Taylor–Galerkin FEM scheme, developed by Löhner et al. [4], and a time-weighted FEM scheme for the semi-implicit governing equations to achieve second-order temporal differencing. Second-order spatial differencing is accomplished by linear unstructured finite element discretization (although strictly speaking, linear unstructured finite elements are spatially second-order only on uniform meshes). For simplicity, this study illustrates the PCICE-FEM development on two-dimensional flow fields. Linear triangular finite elements are used exclusively for the finite element formulations as they are easily generated on domains with complex geometries, they can be easily adapted to minimize error in the solution, and they can be integrated exactly, which eliminates the need of time consuming quadrature integration. The PCICE algorithm could be used with any appropriate

spatial differencing and high-resolution schemes. However, the explicit two-step Taylor–Galerkin FEM [4] combined with flux-corrected transport (FCT), termed the FEM-FCT scheme [5,6], is used as the basis for the explicit predictor phase of PCICE-FEM scheme because of its ability to accurately simulate strong transients (shock wave propagation) involving complex geometries. The PCICE-FEM scheme extends this capability. It also excels on steady-state simulations, including steady-state viscous flows, and is applicable over a much wider Mach number range than the FEM-FCT scheme while maintaining the ability to accurately simulate strong transients.

Expressing the time rate of density change in terms of pressure and energy with the equation of state results in a non-symmetric coefficient matrix for the pressure Poisson equation. For the PCICE-FEM scheme, the preconditioned bi-conjugate gradient stabilized (Bi-CGSTAB) iterative method [7] is used to solve the pressure Poisson equation because of its ability to solve a non-symmetric system of equations and for its smooth convergence. A new Jacobi preconditioner is developed for Bi-CGSTAB based upon the coefficient matrix for the pressure Poisson equation. This new preconditioner has proven to be very efficient for Bi-CGSTAB, requiring only 4–7 iterations to achieve a reduction of four orders of magnitude in the relative error for pressure change.

After stating the governing hydrodynamic equations to be modeled, a complete derivation of the PCICE algorithm is presented. This will include temporal discretization of the governing hydrodynamic equations and the derivation of the three computational phases of the PCICE algorithm. The algorithmic development is followed by an FEM description of the spatial discretization and solution of the three computational phases to complete the development of the PCICE-FEM scheme. The final section presents some solution results and observations regarding this new scheme. These simulations will illustrate the entire range of applicability of the PCICE-FEM scheme, from the near incompressible to highly compressible flow regimes. They include steady and transient, inviscid and viscous simulations. A basis for accuracy is established by simulating flow for which there are known solutions.

2. Governing hydrodynamic equations

The governing hydrodynamic equations considered here are the compressible Euler (inviscid) and Navier–Stokes (viscous) equations. They are defined in two-dimensional, conservative differential form as

$$\frac{\partial U}{\partial t}+\frac{\partial f}{\partial x}+\frac{\partial g}{\partial y}=\frac{\partial f_{\mathrm{v}}}{\partial x}+\frac{\partial g_{\mathrm{v}}}{\partial y}+Q, \tag{1}$$

or in compact conservative differential vector form as

$$\frac{\partial U}{\partial t}+\vec{\nabla}\cdot\vec{F}=\vec{\nabla}\cdot\vec{F}_{\mathrm{v}}+Q. \tag{2}$$

U is the column vector of the conservative variables given by

$$U=\left\{\begin{array}{c}\rho\\ \rho\vec{u}\\ \rho e_{\mathrm{t}}\end{array}\right\}=\left\{\begin{array}{c}\rho\\ \rho u\\ \rho v\\ \rho e_{\mathrm{t}}\end{array}\right\},$$

where ρ is density, u and v are the x and y components of the velocity vector $\vec{u}$, and e_{t} is the specific total energy. In terms of conserved variables, ρu and ρv are the momentum components and ρe_{t} is the total energy. The advective flux vector, $\vec{F}$ in Eq. (2), is defined by its components f and g as

$$f = \begin{Bmatrix} \rho u \\ \rho u^2 + P \\ \rho uv \\ \rho u h_t \end{Bmatrix} \qquad g = \begin{Bmatrix} \rho v \\ \rho uv \\ \rho v^2 + P \\ \rho v h_t \end{Bmatrix},$$

where h_t is the specific total enthalpy, defined by

$$h_t = \frac{\rho e_t + P}{\rho}, \tag{3}$$

and P is the pressure. The viscous flux vector, $\vec{F}_v$ in Eq. (2), is defined by its components f_v and g_v as

$$f_v = \begin{Bmatrix} 0 \\ \tau_{xx} \\ \tau_{xy} \\ u\tau_{xx} + v\tau_{xy} - q_x \end{Bmatrix} \qquad g_v = \begin{Bmatrix} 0 \\ \tau_{xy} \\ \tau_{yy} \\ u\tau_{xy} + v\tau_{yy} - q_y \end{Bmatrix},$$

where τ_{xx}, τ_{xy}, and τ_{yy} are the components of the viscous stress tensor and q_x and q_y are the components of the heat flux vector. Q in Eq. (2) is the column vector of source terms.

While the PCICE algorithm is not restricted to any specific equation of state, the ideal gas equation of state is used throughout the development of the PCICE-FEM scheme for it's simplicity and functional dependence on density and energy,

$$P = (\gamma - 1)\rho e = \rho R_c T. \tag{4}$$

In Eq. (4), e is the specific internal energy, R_c is the gas constant per unit mass of the fluid, and T is the absolute temperature.

3. The PCICE-FEM scheme

In the late 1960s, Harlow and Amsden [1,2] developed the ICE scheme as an "all speed" method. It was the first approach that removed the acoustic component from the Courant stability limitation for compressible flows. For nearly incompressible flows, the ICE scheme essentially reduces to the MAC scheme [8,9]. The original ICE scheme has served as the basis for a number of CFD algorithms and computer programs.

What separates the PCICE-FEM scheme from the original ICE scheme and most other semi-implicit pressure-based schemes is that the full conservative set of governing hydrodynamic equations are solved in predictor–corrector form. Generally, only the momentum equations are solved in this form. The predictor–corrector form of the PCICE algorithm is developed by splitting the implicit and explicit terms of the semi-implicit temporal discretization of the governing hydrodynamic equations into an explicit predictor phase and a semi-implicit pressure-correction phase. These two phases are coupled by the solution of a pressure Poisson equation formed of a strong mass–momentum coupling and somewhat weaker energy coupling. The strong mass–momentum coupling is obtained by substituting the semi-implicit momentum balance equations into the semi-implicit mass conservation equation. The weaker energy coupling is obtained by using an explicit predictor for mass and total energy to express the time rate of density change (in the mass equation) in terms of pressure and energy (through the equation of state). The explicit predictor phase provides the pressure Poisson equation with a sufficient amount of time-advanced information to avoid an iterative solution procedure with the semi-implicit pressure-correction phase.

The development of the PCICE-FEM scheme begins with the semi-implicit temporal discretization of the PCICE algorithm. From this temporal discretization, the derivations of the explicit predictor equations, the pressure Poisson equation, and the semi-implicit pressure-correction equations is then presented. Following these derivations, the finite element spatial discretization, the application of artificial dissipation, and the solution procedures for the three computational phases are given.

3.1. The PCICE algorithm

The ICE coupling procedure eliminates the time-advanced momentum as an unknown. The time-advanced density term is eliminated by employing the equation of state to express density in terms of pressure and energy. Given the general functional form of the equation of state for a compressible fluid, $P = f(\rho, e)$, the differential form with respect to time t is

$$\frac{\partial P}{\partial t} = \left(\frac{\partial P}{\partial \rho}\right)_e \frac{\partial \rho}{\partial t} + \left(\frac{\partial P}{\partial e}\right)_\rho \frac{\partial e}{\partial t}. \tag{5}$$

With Eq. (5), a thermodynamic relationship is defined that can be solved for the density change to eliminate time-advanced density from the pressure Poisson equation. However, the second term on the right hand side of Eq. (5) introduces a time rate dependency on energy. Unfortunately, direct coupling of the conservation form of the total energy equation with the pressure Poisson equation, through the equation of state, is not possible with a semi-implicit scheme because there is no way to eliminate total enthalpy as an unknown in the convective flux term of the total energy equation. To circumvent this problem, the PCICE algorithm incorprates an explicit predictor for total energy to provide Eq. (5) with time-advanced energy information to give the pressure Poisson equation the energy information it requires.

3.1.1. Temporal discretization of the governing hydrodynamic equations

Applying a time-weighted method on the convective fluxes of Eq. (2), the semi-implicit temporal discretization of the governing equations for the PCICE algorithm are as follows:
for the conservation of mass equation

$$\rho^{n+1} = \rho^n - \Delta t \vec{\nabla} \cdot \left[\varphi(\rho\vec{u})^{n+1} + (1-\varphi)(\rho\vec{u})^n\right] + \Delta t s^n, \tag{6}$$

for the balance of momentum equations,

$$(\rho\vec{u})^{n+1} = (\rho\vec{u})^n - \Delta t \vec{\nabla} \cdot \left(\rho\vec{u} \otimes \vec{u}\right)^{n+\varphi} - \Delta t \vec{\nabla}\left[\varphi\bar{P} + (1-\varphi)P^n\right] + \Delta t T_{\mathrm{m}}^n + \Delta t \vec{d}^n, \tag{7}$$

and for the conservation of total energy equation,

$$(\rho e_{\mathrm{t}})^{n+1} = (\rho e_{\mathrm{t}})^n - \Delta t \vec{\nabla} \cdot \left[\varphi(\rho\vec{u})^{n+1}\bar{h}_{\mathrm{t}} + (1-\varphi)(\rho\vec{u})^n h_{\mathrm{t}}^n\right] + \Delta t T_{\mathrm{e}}^n + \Delta t i^n. \tag{8}$$

In Eqs. (6)–(8), s, $\vec{d}$, and i are the mass, momentum, and total energy sources, respectively. T_{m} is the components of the viscous stress force and T_{e} is the viscous heat and heat conduction terms. In Eq. (7), $\bar{P}$ is an approximation of the time-advanced pressure which will be defined in Section 3.1.3 Similarly, the approximation of the time-advanced total enthalpy $\bar{h}_{\mathrm{t}}$ in Eq. (8) will be defined in Section 3.1.4 The superscripts n and $n+1$ denote values at the beginning and the end of a time step, respectively. The time-weighting parameter φ varies between 0.5 and 1.0 and when $\varphi = 0.5$, the convective fluxes are exactly time-centered. Δt is the incremental time step size. An explicit temporal discretization of the momentum

convective flux is required for this semi-implicit formulation. The superscript $n+\varphi$ on the momentum convective flux term of Eq. (7) denotes an *explicit intermediate time* of $t = t^n + \varphi\Delta t$. The PCICE-FEM scheme addresses this term with a modified form of the two-step Taylor–Galerkin FEM scheme [4] (see Section 3.2.1).

3.1.2. The explicit predictor phase

Derivation of the explicit predictor phase equations begins with the momentum balance equations. The explicitly time-advanced momentum is then used in the time-weighted convective fluxes of the explicit predictor equations for mass conservation and total energy. The explicit predictor for momentum balance is Eq. (7) without the time-weighted pressure gradient term. This is the fractional-step form described by Chorin [10] and employed by Harlow and Amsden [2] in the original ICE scheme. The form differs slightly here as the convective flux terms are explicitly time-weighted instead of being evaluated at time t^n. The explicit terms in Eq. (7) are collected to form

$$\delta(\rho\vec{u}) = -\Delta t\vec{\nabla}\cdot\left(\rho\vec{u}\otimes\vec{u}\right)^{n+\varphi} + \Delta t T_{\mathrm{m}}^{n} + \Delta t\vec{d}^{n}. \tag{9}$$

$\delta(\rho\vec{u})$ represents an explicit change in the momentum components for a given time step Δt defined by

$$\delta(\rho\vec{u}) = (\rho\vec{u})^{*} - (\rho\vec{u})^{n}, \tag{10}$$

where $(\rho\vec{u})^{*}$ is the explicit time-advanced momentum approximation. The asterisk * superscript indicates explicit time-advanced values without the application of artificial dissipation.

The explicit predictor equation for mass conservation is formed by collecting the explicit terms resulting from mass–momentum coupling. Rewriting Eq. (7) in terms of Eq. (9) yields

$$(\rho\vec{u})^{n+1} = (\rho\vec{u})^{n} + \delta(\rho\vec{u}) - \Delta t\vec{\nabla}\left[\varphi\bar{P} + (1-\varphi)P^{n}\right]. \tag{11}$$

Substituting Eq. (11) into the implicit convective mass flux term of Eq. (6) yields a precursory form of the pressure Poisson equation,

$$\rho^{n+1} = \rho^{n} - \Delta t\vec{\nabla}\cdot\left[\varphi\delta(\rho\vec{u}) + (\rho\vec{u})^{n}\right] + \Delta t s^{n} + \varphi\Delta t^{2}\vec{\nabla}\cdot\vec{\nabla}\left[\varphi\bar{P} + (1-\varphi)P^{n}\right]. \tag{12}$$

Collecting the explicit mass conservation terms on the right-hand side of Eq. (12) yields the explicit predictor equation for mass conservation,

$$\delta\rho = -\Delta t\vec{\nabla}\cdot\left[\varphi\delta(\rho\vec{u}) + (\rho\vec{u})^{n}\right] + \Delta t s^{n}, \tag{13}$$

where $\delta\rho$ is the explicit change in density for a given time step Δt. $\delta\rho$ is defined by

$$\delta\rho = \rho^{*} - \rho^{n}, \tag{14}$$

where ρ^{*} is the explicit time-advanced density.

The explicit predictor equation for total energy is chosen to be analogous to the explicit predictor for mass conservation. The explicit convective flux for total energy is obtained by multiplying the time-weighted mass flux by the total enthalpy at time t^n. The explicit total energy equation includes the terms for viscous heating, heat conduction, and energy source, all at time t^n. This explicit equation is written as

$$\delta(\rho e_{\mathrm{t}}) = -\Delta t\vec{\nabla}\cdot\left[\varphi\delta(\rho\vec{u}) + (\rho\vec{u})^{n}\right]h_{\mathrm{t}}^{n} + \Delta t T_{\mathrm{e}}^{n} + \Delta t i^{n}, \tag{15}$$

where $\delta(\rho e_t)$ is the explicit change in total energy across a time step Δt. $\delta(\rho e_t)$ is defined by

$$\delta(\rho e_t) = (\rho e_t)^* - (\rho e_t)^n, \tag{16}$$

where $(\rho e_t)^*$ is the explicit time-advanced total energy.

The PCICE-FEM scheme is subject to numerical oscillations of the flow variables in regions of large solution curvature. The explicit predictor phase of the PCICE-FEM scheme concludes with an explicit application of artificial dissipation, or smoothing, of the conserved variables. From this point on, the explicit time-advanced solution variables will be denoted as $\tilde{\rho}$, $\widetilde{\rho\vec{u}}$, and $\widetilde{\rho e}_t$ with the tilde ˜ indicating that the explicit solution variables from Eqs. (10), (14), and (16) have been smoothed with an artificial dissipation method. Upon smoothing,

$$(\rho\vec{u})^* \to \widetilde{\rho\vec{u}}, \quad \rho^* \to \tilde{\rho}, \quad (\rho e_t)^* \to \widetilde{\rho e}_t. \tag{17}$$

Adding artificial dissipation completes the explicit predictor phase of the PCICE algorithm. After the explicit flow variables have been smoothed with artificial dissipation, the pressure Poisson equation is assembled from these smoothed components. The application of artificial dissipation for the explicit predictor phase variables is covered in Section 3.2.4.

3.1.3. The pressure Poisson equation

The derivation of the pressure Poisson equation for the PCICE algorithm begins with Eq. (11) rewritten in terms of the smoothed explicit change in the momentum components,

$$(\rho\vec{u})^{n+1} = (\rho\vec{u})^n + \delta(\widetilde{\rho\vec{u}}) - \Delta t\vec{\nabla}\left[\varphi\bar{P} + (1-\varphi)P^n\right], \tag{18}$$

where $\delta(\widetilde{\rho\vec{u}})$ is defined as

$$\delta(\widetilde{\rho\vec{u}}) = \widetilde{\rho\vec{u}} - (\rho\vec{u})^n. \tag{19}$$

Eq. (18) is the semi-implicit pressure correction equation for momentum and is discussed in Section 3.1.4.

Substituting Eq. (18) into Eq. (6) to eliminate $(\rho\vec{u})^{n+1}$ as an unknown, yields the pressure Poisson equation in terms of implicit density and pressure,

$$\rho^{n+1} - \rho^n = -\Delta t\vec{\nabla}\cdot\left[\varphi\delta(\widetilde{\rho\vec{u}}) + (\rho\vec{u})^n\right] + \Delta t s^n + \varphi\Delta t^2\vec{\nabla}\cdot\vec{\nabla}\left[\varphi\bar{P} + (1-\varphi)P^n\right]. \tag{20}$$

For Harlow and Amsden's [2] original ICE scheme, the equation of state neglected the dependence of pressure on internal energy. Therefore, only time-advanced pressure was introduced into the pressure Poisson equation with the equation of state substitution. However, direct incorporation of Eq. (5) into the pressure Poisson equation introduces a dependence on internal energy. If the internal energy term of Eq. (5) is addressed at time t^{n+1}, then an iterative procedure between the pressure Poisson equation and the semi-implicit governing equations has to be implemented. Westbrook [11] addressed this problem with the development of a generalized ICE scheme for combustion simulations where the equation of state allows for the pressure dependency upon internal energy and chemical kinetics to be taken into account. His iterative ICE scheme compares the time-advanced pressure obtained from the pressure Poisson equation to the time-advanced pressure computed from the equation of state to determine convergence. On the other hand, if the internal energy variables of Eq. (5) are sufficiently predicted (as with our PCICE algorithm), the iterative procedure may be avoided.

For simplicity, we will employ the ideal gas equation of state, Eq. (4), in the general form of Eq. (5) to express the left-hand side of Eq. (20) in terms of pressure. Differencing Eq. (5) in terms of temperature, yields

$$P^{n+1} - P^n = R_c\hat{T}(\rho^{n+1} - \rho^n) + R_c\hat{\rho}(T^{n+1} - T^n). \tag{21}$$

The terms with the hat character $\hat{}$ in Eq. (21) denote state variables that may be at any time level between t^n and t^{n+1}.

The procedure developed for the PCICE algorithm is to replace the implicit energy, expressed in Eq. (21) by T^{n+1}, and the state variables with the explicit predictor variables. The implicit pressure P^{n+1} then becomes a linear combination (hybrid) of implicit density and explicit variables. It is convenient to maintain Harlow and Amsden's original ICE notation for the hybrid pressure variable. Eq. (21) in terms of the hybrid pressure $\bar{P}$ then becomes

$$\bar{P} - P^n = R_c\hat{T}(\rho^{n+1} - \rho^n) + R_c\hat{\rho}(\tilde{T} - T^n), \tag{22}$$

where the state variables are defined in the time-weighted manner consistent with the PCICE algorithm,

$$\hat{T} = \varphi\tilde{T} + (1 - \varphi)T^n$$

and

$$\hat{\rho} = \varphi\tilde{\rho} + (1 - \varphi)\rho^n.$$

At this point, a decision must be made whether to express the dependent variable of the pressure Poisson equation as the time-advanced hybrid pressure or as a pressure change. For the PCICE algorithm, the change-in-pressure form was chosen for ease in applying Dirichlet boundary conditions in the iterative Poisson solver (see Section 3.3.3). Introducing the *pressure change variable* as

$$\delta P = \varphi(\bar{P} - P^n), \tag{23}$$

Eq. (20) is recast into the form of

$$\rho^{n+1} - \rho^n = -\Delta t\vec{\nabla}\cdot\left[\varphi\delta(\widetilde{\rho\vec{u}}) + (\rho\vec{u})^n\right] + \Delta ts^n + \varphi\Delta t^2\vec{\nabla}\cdot\vec{\nabla}(\delta P + P^n). \tag{24}$$

Similarly expressed in terms of δP, Eq. (22) becomes

$$\frac{\delta P}{\varphi} = R_c\hat{T}(\rho^{n+1} - \rho^n) + R_c\hat{\rho}(\tilde{T} - T^n). \tag{25}$$

Combining Eq. (25) with (24) to eliminate the density change across a time step, the final form of the pressure Poisson equation for the PCICE algorithm is

$$\frac{\delta P}{\varphi R_c\hat{T}} - \varphi\Delta t^2\vec{\nabla}\cdot\vec{\nabla}\delta P = \frac{\hat{\rho}}{\hat{T}}(\tilde{T} - T^n) - \Delta t\vec{\nabla}\cdot\left[\varphi\delta(\widetilde{\rho\vec{u}}) + (\rho\vec{u})^n\right] + \Delta ts^n + \varphi\Delta t^2\vec{\nabla}\cdot\vec{\nabla}P^n. \tag{26}$$

Eq. (26) is in terms of the one unknown dependent variable, δP. The right-hand side is constructed of explicit terms only, so there is no need to iterate with the semi-implicit governing equations.

3.1.4. The pressure-correction equations

The pressure-correction equations for the PCICE algorithm are derived by subtracting the explicit predictor phase equations (that are expressed in terms of the smoothed variables) from the semi-implicit governing equations. The derivation begins by considering the semi-implicit momentum balance equations, Eq. (18). Note that this equation is already in pressure-correction form. The only implicit variable on the right-hand side of Eq. (18) is the hybrid pressure obtained from the solution of the pressure Poisson

equation. By recasting Eq. (18) in terms of δP, the pressure-correction equation for the momentum components is

$$(\rho\vec{u})^{n+1} = \widetilde{\rho\vec{u}} - \Delta t\vec{\nabla}(\delta P + P^n). \tag{27}$$

The correction equation for mass conservation is derived by subtracting Eq. (13), in terms of smoothed density $\tilde{\rho}$, from Eq. (6), yielding

$$\rho^{n+1} = \tilde{\rho} - \varphi\Delta t\vec{\nabla}\cdot\left[(\rho\vec{u})^{n+1} - \widetilde{\rho\vec{u}}\right]. \tag{28}$$

Unlike the original ICE scheme [2], where the equation of state was employed to correct density, the correction term on the right-hand side of Eq. (28) is essentially the right-hand side of the pressure Poisson equation, Eq. (24). The correction for density given by the equation of state, Eq. (22), is essentially the left-hand side of Eq. (24). Both of these correction approaches for density should be mathematically equivalent. However, from a numerical standpoint, they are applied in very different manners. A correction equation derived from an equation of state is an algebraic equation applied at a point. The correction equation given by Eq. (28) requires spatial discretization. Both of these correction approaches for mass were evaluated for the PCICE-FEM scheme with the correction approach of Eq. (28) giving superior results. Eq. (28) has the advantage of satisfying mass conservation without the time-advanced energy requirements.

The correction equation for total energy is derived by subtracting Eq. (15), in terms of smoothed explicit total energy $\widetilde{\rho e}_t$, from Eq. (8) to give

$$(\rho e_t)^{n+1} = \widetilde{\rho e}_t - \varphi\Delta t\vec{\nabla}\cdot\left[(\rho\vec{u})^{n+1}\bar{h}_t - \widetilde{\rho\vec{u}h}_t^n\right], \tag{29}$$

where the time-advanced total enthalpy is now defined as

$$\bar{h}_t = \frac{\widetilde{\rho e}_t + \bar{P}}{\rho^{n+1}}. \tag{30}$$

3.1.5. The PCICE algorithmic steps

The algorithmic steps for the PCICE algorithm are as follows:

(1) Beginning of time step.

Explicit Predictor

(2) Explicitly determine time-weighted values of $\rho^{n+\varphi}$ and $(\rho\vec{u})^{n+\varphi}$.
(3) Solve Eq. (9) for $\delta(\rho\vec{u})$, and $(\rho\vec{u})^*$.
(4) Solve Eq. (13) for $\delta\rho$ and ρ^*.
(5) Solve Eq. (15)for $\delta(\rho e_t)$, and $(\rho e_t)^*$.
(6) Apply artificial dissipation to smooth the explicit components ρ^*, $(\rho\vec{u})^*$, and $(\rho e_t)^*$ to give $\tilde{\rho}$, $\widetilde{\rho\vec{u}}$, and $\widetilde{\rho e}_t$.
(7) Determine the smoothed explicit pressure and temperature fields, $\tilde{P}$ (predictor for the Poisson solver) and $\tilde{T}$ using the equation of state.

Elliptic pressure Poisson solution

(8) Solve the pressure Poisson Eq. (26) for δP.
(9) Compute the hybrid pressure field $\bar{P}$ from δP using Eq. (23),

Semi-implicit pressure correction

(10) Solve Eq. (27) to obtain $(\rho\vec{u})^{n+1}$.
(11) Solve Eq. (28) to obtain ρ^{n+1}.

(12) Solve Eq. (29) to obtain $(\rho e_t)^{n+1}$.
(13) Calculate P^{n+1} and T^{n+1} and all other necessary thermodynamic variables from the equation of state.
(14) Next time step.

3.2. Explicit predictor phase finite element discretization and solution

This section discusses the finite element discretization and solution of the explicit predictor phase for the PCICE-FEM scheme, including the application of artificial dissipation that may be necessary to stabilize the solution.

3.2.1. Finite element discretization of the explicit predictor for the momentum balance equations

A modified form of the two-step Taylor–Galerkin FEM scheme [4] is employed in the PCICE-FEM scheme to solve the explicit predictor equations for momentum balance. The original two-step form, which is evaluated at $t^{n+1/2} = t^n + \Delta t/2$, is generalized in our modified form to be evaluated around time $t^{n+\varphi} = t^n + \varphi\Delta t$. The spatial discretization of the modified form is identical to the original form. Because $(\rho\vec{u})^{n+\varphi}$ and $\rho^{n+\varphi}$ are needed to obtain $\vec{u}^{n+\varphi}$ for the momentum convective flux term of Eq. (9), the modified first step is used to solve both the momentum balance and mass conservation equations at time $t^{n+\varphi}$.

The modified temporal discretization for the first step of the two-step Taylor–Galerkin FEM scheme is

$$U^{n+\varphi} = U^n - \varphi\Delta t\vec{\nabla}\cdot\vec{F}^n + \varphi\Delta t Q^n. \tag{31}$$

Using the same finite element spatial discretization as the first step of the original two-step Taylor–Galerkin FEM scheme, the first step of the predictor phase for momentum is

$$\Omega_E U_E^{n+\varphi} = \int_\Omega [N]\,\mathrm{d}\Omega\{U\}^n - \varphi\Delta t\int_\Omega [\vec{\nabla}N]\cdot\mathrm{d}\Omega\{\vec{F}\}^n + \varphi\Delta t\Omega_E Q^n, \tag{32}$$

where Ω_E is the volume of element E and $U_E^{n+\varphi}$ is the time-weighted elemental solution. $[N]$ represents the elemental interpolation functions associated with element E. The components of $U_E^{n+\varphi}$ are

$$U_E^{n+\varphi} = \left\{\begin{array}{c}\rho\\ \rho u\\ \rho v\end{array}\right\}_E^{n+\varphi}$$

and the vector components of $\vec{F}^n$ in the x- and y-directions are

$$f^n = \left\{\begin{array}{c}\rho u\\ \rho u^2\\ \rho uv\end{array}\right\}^n \qquad g^n = \left\{\begin{array}{c}\rho v\\ \rho uv\\ \rho v^2\end{array}\right\}^n,$$

respectively.

The modified temporal discretization for the second step of the two-step Taylor–Galerkin FEM scheme is

$$U^{n+1} = U^n - \Delta t\vec{\nabla}\cdot\vec{F}^{n+\varphi} + \Delta t\vec{\nabla}\cdot\vec{F}_v^n + \Delta t Q^n. \tag{33}$$

The convective fluxes of Eq. (33) at time $t^{n+\varphi}$ are determined from the solution of Eq. (32). With these elemental convective fluxes denoted by $\vec{F}_e^{n+\varphi}$, the FEM discretized second step of the momentum balance explicit predictor is

$$\sum_e \int_\Omega \{N\}[N]\mathrm{d}\Omega\{\delta U\} = \Delta t \sum_e \int_\Omega \{\vec{\nabla} N\}\mathrm{d}\Omega \cdot \vec{F}_{\mathrm{e}}^{n+\varphi} - \Delta t \sum_e \int_\Gamma \{N\}\mathrm{d}\Gamma\vec{\eta} \cdot \vec{F}_{\mathrm{e}}^{n+\varphi} - \Delta t \sum_e \int_\Omega \{\vec{\nabla} N\}\mathrm{d}\Omega \cdot \vec{F}_{\mathrm{v}}^{n} + \Delta t \sum_e \int_\Gamma \{N\}\mathrm{d}\Gamma\vec{\eta} \cdot \vec{F}_{\mathrm{v}}^{n} + \Delta t \sum_e \int_\Omega \{N\}\mathrm{d}\Omega Q_{\mathrm{e}}^{n}, \tag{34}$$

where Γ defines the boundary of the domain and $\vec{\eta}$ is the unit vector normal to the boundary. The components of δU are

$$\delta U = \left\{ \begin{array}{c} \delta(\rho u) \\ \delta(\rho v) \end{array} \right\} = \left\{ \begin{array}{c} \rho u^* - \rho u^n \\ \rho v^* - \rho v^n \end{array} \right\}.$$

The elemental vector components of $\vec{F}_{\mathrm{e}}^{n+\varphi}$ in the x- and y-directions are

$$f_{\mathrm{e}}^{n+\varphi} = \left\{ \begin{array}{c} \rho u^2 \\ \rho uv \end{array} \right\}_e^{n+\varphi} \qquad g_{\mathrm{e}}^{n+\varphi} = \left\{ \begin{array}{c} \rho uv \\ \rho v^2 \end{array} \right\}_e^{n+\varphi},$$

respectively. The vector components of the viscous flux vector $\vec{F}_{\mathrm{v}}^{n}$ in the x- and y-directions for the momentum balance, defined in Eq. (2), are

$$f_{\mathrm{v}}^{n} = \left\{ \begin{array}{c} \tau_{xx} \\ \tau_{xy} \end{array} \right\}^n \qquad g_{\mathrm{v}}^{n} = \left\{ \begin{array}{c} \tau_{xy} \\ \tau_{yy} \end{array} \right\}^n,$$

respectively. Q_{e}^{n} are the elemental components of the momentum sources.

3.2.2. Finite element discretization of the explicit predictor for the mass conservation and total energy equations

For the PCICE-FEM scheme, both the explicit mass conservation and the total energy equations, Eqs. (13) and (15), are solved in the form of

$$\delta U = -\Delta t \vec{\nabla} \cdot \vec{F}^* + \Delta t \vec{\nabla} \cdot \vec{F}_{\mathrm{v}}^{n} + \Delta t Q^n, \tag{35}$$

where δU is defined as

$$\delta U = \left\{ \begin{array}{c} \delta\rho \\ \delta(\rho e_{\mathrm{t}}) \end{array} \right\} = \left\{ \begin{array}{c} \rho^* - \rho^n \\ (\rho e_{\mathrm{t}})^* - (\rho e_{\mathrm{t}})^n \end{array} \right\}.$$

$\vec{F}^*$ is the explicit time-weighted convective fluxes,

$$\vec{F}^* = \left\{ \begin{array}{c} \varphi\delta(\rho\vec{u}) + (\rho\vec{u})^n \\ [\varphi\delta(\rho\vec{u}) + (\rho\vec{u})^n]h_{\mathrm{t}}^n \end{array} \right\} = \left\{ \begin{array}{c} \varphi(\rho\vec{u})^* + (1-\varphi)(\rho\vec{u})^n \\ [\varphi(\rho\vec{u})^* + (1-\varphi)(\rho\vec{u})^n]h_{\mathrm{t}}^n \end{array} \right\}.$$

In the x- and y-directions, these convective fluxes are

$$f^* = \left\{ \begin{array}{c} \varphi\delta(\rho u) + (\rho u)^n \\ [\varphi\delta(\rho u) + (\rho u)^n]h_{\mathrm{t}}^n \end{array} \right\} \qquad g^* = \left\{ \begin{array}{c} \varphi\delta(\rho v) + (\rho v)^n \\ [\varphi\delta(\rho v) + (\rho v)^n]h_{\mathrm{t}}^n \end{array} \right\},$$

respectively. The vector components of the viscous flux vector $\vec{F}_{\mathrm{v}}^{n}$ in the x- and y-directions for mass and total energy, defined in Eq. (2), are

$$f_{\mathrm{v}}^{n} = \left\{ \begin{array}{c} 0 \\ u\tau_{xx} + v\tau_{xy} - q_x \end{array} \right\}^n \qquad g_{\mathrm{v}}^{n} = \left\{ \begin{array}{c} 0 \\ u\tau_{xy} + v\tau_{yy} - q_y \end{array} \right\}^n,$$

respectively. Q^n of Eq. (35) are the mass conservation and total energy sources. The finite element discretization of the explicit predictor equations for mass conservation and total energy is

$$\sum_e \int_\Omega \{N\}[N]\mathrm{d}\Omega\{\delta U\} = \Delta t \sum_e \int_\Omega \{N\}[\vec{\nabla} N]\mathrm{d}\Omega \cdot \{\vec{F}^*\} - \Delta t \sum_e \int_\Gamma \{N\}[N]\mathrm{d}\Gamma\vec{\eta} \cdot \{\vec{F}^*\} - \Delta t \sum_e \int_\Omega \{\vec{\nabla} N\}\mathrm{d}\Omega \cdot \vec{F}^n_{\mathrm{v}} + \Delta t \sum_e \int_\Gamma \{N\}\mathrm{d}\Gamma\vec{\eta} \cdot \vec{F}^n_{\mathrm{v}} + \Delta t \sum_e \int_\Omega \{N\}\mathrm{d}\Omega Q^n_{\mathrm{e}}. \tag{36}$$

Eqs. (34) and (36) contain boundary integrals for the convective flux vector and the viscous stress tensor. The approach for the viscous boundary integral is the same approach employed in the two-step Taylor–Galerkin FEM scheme [12]. This approach applies the same elemental viscous flux determined in the interior of the element on the boundary face. To approximate the terms of the convective flux vector on the boundary, the procedure for the PCICE-FEM scheme is to forward-time discretize themass conservation and fractional momentum equations in the boundary normal direction. A discretized energy equation at the boundary is not needed because the total enthalpy variable in Eq. (35) is at time t^n.

3.2.3. Solution of the explicit predictor equations

For the PCICE-FEM scheme, Eqs. (34) and (36), are each cast in the compact symbolic form of

$$M_{\mathrm{c}}\,\delta U = R, \tag{37}$$

where δU is the change in explicit variables and M_{c} denotes the consistent mass matrix formed from

$$M_{\mathrm{c}} = \sum_e \int_\Omega \{N\}[N]\mathrm{d}\Omega.$$

In Eq. (37), R is the vector of added element contributions defined by the right hand side of Eqs. (34) and (36).

Eq. (37) can be solved efficiently with an iterative procedure developed by Donea [13] in which it is recast as

$$M_{\mathrm{l}}\,\delta U + M_{\mathrm{c}}\,\delta U = R + M_{\mathrm{l}}\,\delta U, \tag{38}$$

where M_{l} denotes the lumped mass matrix. In iterative form, Eq. (38) becomes

$$M_{\mathrm{l}}\,\delta U_{i+1} = R + \varepsilon(M_{\mathrm{l}} - M_{\mathrm{c}})\delta U_i, \quad i = 1, 2, \ldots, N_{\mathrm{iter}}, \tag{39}$$

where N_{iter} is the number of iterations. Three iterations is sufficient for convergence. The parameter ε is set to $\varepsilon = 1$ for transient simulations. For steady-state solutions, the number of time steps can be reduce by implementing residual smoothing [14]. This is accomplished by setting ε to a small negative number. Typically for steady-state simulations, $\varepsilon = -0.1$, but this value is somewhat problem dependent. A negative ε renders the second term on the right-hand side of Eq. (39) diffusive. This elliptic character adds a certain level of implicitness to Eq. (39). The maximum allowable time step can then be slightly increased. Notice that the elliptic effect vanishes at steady-state where $\delta U = 0$.

3.2.4. Application of artificial dissipation for the components of the explicit predictor phase of the PCICE-FEM scheme

After the explicit predictor equations have been solved, artificial dissipation is applied through either a variable diffusion method or a high-resolution scheme to smooth the non-physical numerical oscillations in the flow variables. For the PCICE-FEM scheme, the variable diffusion is a pressure-sensed method of

Swanson and Turkel [15] and the high-resolution scheme is an improved version of Löhner's flux-corrected transport (FCT) scheme [5,6].

The Swanson and Turkel [15] artificial dissipation method incorporates a weighted combination of Peraire's artificial dissipation method [16] and Jameson's classic artificial viscosity method [17]. Both Peraire's and Jameson's methods incorporate a diffusion coefficient based upon the second derivative of pressure. The pressure sensor for the method of Swanson and Turkel in finite element form [18] is

$$S_{\mathrm{p}} = \frac{\sum_e |2P_I - P_J - P_K|}{\sum_e [\alpha(|P_I - P_J| + |P_J - P_K|) + (1-\alpha)\underline{P}]}, \tag{40}$$

where α is the weighting parameter, $\underline{P}$ is the average elemental pressure, and I, J, K refers to the local nodes numbers of element e. In a finite element context, this artificial dissipation method is applied to the conserved flow variables with

$$\tilde{U} = U^* + C_{\mathrm{p}} M_{\mathrm{l}}^{-1}\left[S_{\mathrm{p}}(M_{\mathrm{c}} - M_{\mathrm{l}})\{U^h\}\right], \tag{41}$$

where C_{p} is a user specified constant typically ranging between 0.1 and 0.5.

An improvement to Löhner's FEM-FCT scheme [5,6] for the solution of hydrodynamic conservation equations was developed by Georghiou et al. [19]. Georghiou uses the same high and low-order schemes that were developed by Löhner. However, where Löhner employed a globally constant diffusion coefficient of $C_{\mathrm{d}} = 1.0$, Georghiou's modification employs a globally varying diffusion coefficient. This new diffusion coefficient is assumed to be constant in each element and renders the low-order scheme equivalent to a first-order upwind scheme which has the minimum amount of diffusion required to ensure monotonic results. The form of the new elemental diffusion coefficient is

$$C_{\mathrm{d}} = \frac{C_{\mathrm{e}}(1.0 - C_{\mathrm{e}})}{2}. \tag{42}$$

In Eq. (42), C_{e} is the elemental material Courant number defined by

$$C_{\mathrm{e}} = \frac{|\vec{u}_{\mathrm{e}}|\Delta t}{h_{\mathrm{e}}},$$

where $|\vec{u}_{\mathrm{e}}|$ is the magnitude of the elemental velocity and h_{e} is the minimum elemental length.

3.3. Pressure Poisson equation finite element discretization and solution

In this section we describe the finite element spatial discretization and solution of the pressure Poisson equation incorporated into the PCICE-FEM scheme. The spatial discretization with the standard Galerkin finite element method is presented and boundary conditions for the pressure Poisson equation that are consistent with the finite element spatial discretization and the physics of the governing hydrodynamic equations are then developed. We conclude this section with a description of the preconditioned Bi-CGSTAB iterative method with a new Jacobi preconditioner for solving the pressure Poisson equation.

3.3.1. Pressure Poisson equation finite element discretization

The standard Galerkin finite element method discretization of the pressure Poisson equation, Eq. (26), is

$$\sum_e \int_\Omega \{N\}[N]\mathrm{d}\Omega\left[\frac{1}{\varphi R_c \hat{T}}\right]\{\delta P\} + \varphi\Delta t^2 \sum_e \int_\Omega \{\vec{\nabla}N\}\cdot[\vec{\nabla}N]\mathrm{d}\Omega\{\delta P\} - \varphi\Delta t^2 \sum_e \int_\Gamma \{N\}\mathrm{d}\Gamma \frac{\partial(\delta P)}{\partial\vec{\eta}}$$
$$= \sum_e \int_\Omega \{N\}[N]\mathrm{d}\Omega\left\{\frac{\hat{\rho}}{\hat{T}}(\tilde{T} - T^n)\right\} + \Delta t \sum_e \int_\Omega \{\vec{\nabla}N\}[N]\mathrm{d}\Omega\cdot\{(\widetilde{\rho\vec{u}})^{n+\varphi}\}$$
$$- \Delta t \sum_e \int_\Gamma \{N\}[N]\mathrm{d}\Gamma\{(\widetilde{\rho u}_\eta)^{n+\varphi}\} + \Delta t \sum_e \int_\Omega \{N\}\mathrm{d}\Omega s_e^n$$
$$- \varphi\Delta t^2 \sum_e \int_\Omega \{\vec{\nabla}N\}\cdot[\vec{\nabla}N]\mathrm{d}\Omega\{P^n\} + \varphi\Delta t^2 \sum_e \int_\Gamma \{N\}\mathrm{d}\Gamma \frac{\partial P^n}{\partial\vec{\eta}}. \tag{43}$$

In Eq. (43), the explicit time-weighted convective mass flux is defined as

$$(\widetilde{\rho\vec{u}})^{n+\varphi} = \varphi\delta(\widetilde{\rho\vec{u}}) + (\rho\vec{u})^n. \tag{44}$$

3.3.2. Boundary conditions for the pressure Poisson equation

The spatial integration of the pressure Poisson equation derived for the PCICE-FEM scheme results in a set of boundary conditions that are not typically found in the governing hydrodynamic equations describing a fluid continuum. Eq. (43) contains boundary integrals requiring knowledge of the normal pressure gradients for both the time-advanced hybrid pressure $\bar{P}$, in terms of δP, and the old-time pressure P^n. These normal pressure gradients, commonly referred to as Neumann boundary conditions, are generally unknown. Not only are they unknown, but a characteristic analysis of the governing hydrodynamic equations for compressible flow shows that the normal pressure gradient on a boundary is never to be specified. The characteristic analysis shows that either the pressure or the velocity (but not both, except on a supersonic inlet) must be specified for subsonic flow boundaries. While an analysis of the governing hydrodynamic equations may determine what the normal pressure gradients should be near an inflow or outflow boundary, the application of the normal pressure gradient is not a requirement to achieve a unique solution and may be considered redundant. At a stationary solid wall where the mass flux is specified to be zero, it can be effectively argued that the additional specification of the normal pressure gradient overspecifies the boundary. Therefore, the correct boundary conditions for the pressure Poisson equation require the application of Dirichlet boundary conditions for δP or the specification of momentum in the normal direction as a Neumann boundary condition.

Gresho and Sani [20,21] give an extensive discussion of the problems created with the introduction of normal pressure gradient boundary conditions (Neumann) for incompressible flows. They state that the Neumann boundary condition is always appropriate for the pressure Poisson equation, for both the set of initial conditions and at solution times greater than zero. However, what they call a Neumann boundary condition is the result of replacing the normal pressure gradient at the boundary with the normal momentum equation applied at the boundary. Thus, all of the Neumann boundary conditions in the forcing function of the pressure Poisson equation are in terms of velocity. This is precisely the approach utilized here for the PCICE-FEM scheme. Veldman [22] summarized this approach as "first discretize the equations of motion, next substitute the original boundary conditions, and finally combine the discrete equations."

The first step in applying Gresho and Sani's approach to constructing an appropriate set of Neumann boundary conditions for the pressure Poisson equation is to write the semi-implicit momentum balance equations in terms of the boundary variables found in Eq. (43). Multiplying Eq. (27) by φ and substituting Eq. (44) gives

$$(\rho\vec{u})^{n+\varphi} = (\widetilde{\rho\vec{u}})^{n+\varphi} - \varphi\Delta t\vec{\nabla}(\delta P + P^n), \tag{45}$$

where the left-hand side of Eq. (45) is written in terms of the implicit time-weighted momentum variable defined as

$$(\rho\vec{u})^{n+\varphi} = \varphi(\rho\vec{u})^{n+1} + (1-\varphi)(\rho\vec{u})^{n}.$$

Eq. (45) is now substituted into Eq. (43) to give

$$\begin{aligned}
&\sum_e \int_\Omega \{N\}[N]\mathrm{d}\Omega\left[\frac{1}{\varphi R_c \hat{T}}\right]\{\delta P\} + \varphi\Delta t^2 \sum_e \int_\Omega \{\vec{\nabla}N\}\cdot[\vec{\nabla}N]\mathrm{d}\Omega\{\delta P\} \\
&\quad = \sum_e \int_\Omega \{N\}[N]\mathrm{d}\Omega\left\{\frac{\hat{\rho}}{\hat{T}}(\tilde{T}-T^n)\right\} + \Delta t \sum_e \int_\Omega \{\vec{\nabla}N\}[N]\mathrm{d}\Omega\cdot\{(\widetilde{\rho\vec{u}})^{n+\varphi}\} \\
&\qquad - \Delta t \sum_e \int_\Gamma \{N\}[N]\mathrm{d}\Gamma\{(\rho u_\eta)^{n+\varphi}\} + \Delta t \sum_e \int_\Omega \{N\}\mathrm{d}\Omega s_e^n - \varphi\Delta t^2 \sum_e \int_\Omega \{\vec{\nabla}N\}\cdot[\vec{\nabla}N]\mathrm{d}\Omega\{P^n\}. \quad (46)
\end{aligned}$$

Eq. (46) is the final form of the discretized pressure Poisson equation for the PCICE-FEM scheme. Note that the normal pressure gradient boundary integrals have been eliminated. The Neumann boundary condition is now satisfied through the convective mass flux boundary integral. Dirichlet boundary conditions are applied through the specification of δP. Therefore, along the boundary, either the normal component of the implicit time-weighted mass flux, $(\rho\vec{u})^{n+\varphi}$, or the implicit change in pressure, δP, must be specified in order to solve Eq. (46).

3.3.3. Solving the pressure Poisson equation with Bi-CGSTAB

The discretized pressure Poisson equation for the PCICE-FEM scheme requires the solution of a linear algebraic system of equations in which the coefficient matrix is sparse and non-symmetric. The preconditioned Bi-CGSTAB iterative method [7] is used to solve the discretized pressure Poisson equation. We develop a Jacobi preconditioning matrix based upon the coefficient matrix for the PCICE-FEM scheme pressure Poisson equation. With this new diagonal preconditioning matrix and exact finite element integration, no matrix storage is required by Bi-CGSTAB, only the assembly of matrix-vector dot products.

Eq. (46) may be written in the standard form of an algebraic system of equations,

$$Ax = b. \quad (47)$$

In Eq. (47), x is the solution vector composed of nodal values of δP. The coefficient matrix A is defined by

$$A = \sum_e \int_\Omega \{N\}[N]\mathrm{d}\Omega\left[\frac{1}{\varphi R_c \hat{T}}\right] + \varphi\Delta t^2 \sum_e \int_\Omega \{\vec{\nabla}N\}\cdot[\vec{\nabla}N]\mathrm{d}\Omega \quad (48)$$

and b is the forcing vector defined by the right hand side of Eq. (46).

Using van der Vorst's [7] notation, the Bi-CGSTAB algorithm is as follows:

x_0 is an initial guess;
$r_0 = b - Ax_0$
$\rho_0 = \alpha = \omega_0 = 1$;
$v_0 = p_0 = 0$;
for $i = 1, 2, 3, \ldots$;
$\rho_i = (r_0, r_{i-1})$;
$\beta = (\rho_i/\rho_{i-1})(\alpha/\alpha\omega_{i-1})$;
$p_i = r_{i-1} + \beta(p_{i-1} - \omega_{i-1}v_{i-1})$;
Solve y from $Ky = p_i$;
$v_i = Ay$;

$\alpha = r_i/(r_0, v_i)$;
$s = r_{i-1} - \alpha v_i$;
Solve z from $Kz = s$;
$t = Az$;
$\omega_i = (t, s)/(t, t)$;
$x_i = x_{i-1} + \alpha y + \omega_i z$;
if x_i is accurate enough, then stop;
$r_i = s - \omega_i t$;
end

The initial estimate for the solution vector comes from the explicit predictor for pressure, $x_0 = \varphi(\tilde{P} - P^n)$. Dirichlet boundary conditions are strongly enforced on y, z, and x_i. This is a simple procedure as $\delta P = 0$ (thus $y = z = x_i = 0$) for a constant pressure boundary.

The matrix K in the above algorithm is the preconditioning matrix. The preconditioning matrix for the PCICE-FEM scheme is derived from the two sub-matrices of A,

$$M^\rho = \sum_e \int_\Omega \{N\}[N]\mathrm{d}\Omega\left[\frac{1}{\varphi R_c \hat{T}}\right]$$

and

$$K^\rho = \varphi\Delta t^2 \sum_e \int_\Omega \{\vec{\nabla}N\} \cdot [\vec{\nabla}N]\mathrm{d}\Omega.$$

The new Jacobi preconditioning matrix for the PCICE-FEM scheme is the lumped-mass form of M^ρ plus the diagonal of K^ρ,

$$K = M_l^\rho + \mathrm{diag}\, K^\rho. \tag{49}$$

This new preconditioning matrix allows convergence of the Bi-CGSTAB algorithm in 4–7 iterations to achieve a reduction of four orders of magnitude in the relative error for pressure change.

3.4. Finite element discretization and solution of the pressure-correction equations

The final phase of the PCICE algorithm is the pressure-correction of the flow variables from the explicit predictor phase. In the PCICE-FEM scheme, the pressure-correction equations are spatially discretized with the standard Galerkin FEM. Eqs. (27)–(29) are solved in successive order so that all of the right-hand side terms are known nodal quantities. Thus, integration by parts is not necessary because the boundary conditions are already satisfied and there is no problem with differentiability constraints for nodal values.

Eqs. (27)–(29) are recast in correction form as

$$U' = -\Delta t\vec{\nabla} \cdot \vec{F}', \tag{50}$$

where

$$U' = \begin{Bmatrix} \rho^{n+1} - \tilde{\rho} \\ (\rho\vec{u})^{n+1} - \widetilde{\rho\vec{u}} \\ (\rho e_t)^{n+1} - \widetilde{\rho e}_t \end{Bmatrix} \qquad \vec{F}' = \begin{Bmatrix} \varphi[(\rho\vec{u})^{n+1} - \widetilde{\rho\vec{u}}] \\ \delta P + P^n \\ \varphi[(\rho\vec{u})^{n+1}\bar{h}_t - \widetilde{\rho\vec{u}h_t^n}] \end{Bmatrix}.$$

U' and $\vec{F}'$ are the correction variables and correction fluxes, respectively. Applying the standard Galerkin FEM to Eq. (50), yields the finite element discretized correction equation,

$$\sum_e \int_\Omega \{N\}[N]\mathrm{d}\Omega\{U'\} = -\Delta t \sum_e \int_\Omega \{N\}[\vec{\nabla}N]\mathrm{d}\Omega \cdot \{\vec{F}'\}. \tag{51}$$

To solve the discretized correction equations, Eq. (51) is cast in the form of Eq. (37) and iteratively solved with Eq. (39).

3.5. Stability of the PCICE-FEM scheme

An in-depth stability analysis was not performed for the PCICE-FEM scheme. Typically, these stability analyzes are performed upon linear systems of equations and are approximations at best. It was expected that, because the two-step Taylor–Galerkin FEM scheme [4] is the basis for the explicit predictor for the momentum balance, the coefficient in the stability criteria would remain the same. The time step size criteria employed for the PCICE-FEM scheme is

$$\Delta t \leqslant \frac{\alpha\beta h_\mathrm{e}}{|\vec{u}|} \tag{52}$$

for $\varphi \geqslant 0.5$. In Eq. (52), $|\vec{u}|$ is the magnitude of the local velocity, α is a dimensionless parameter that is determined by a linear stability analysis, and β is a user defined factor of safety. This stability criteria works quite well when simulating inviscid flows. A stability coefficient of $\alpha = 0.5$ and a safety factor of $\beta = 0.8$–0.9 are the parameters used for transient inviscid simulations. The safety factor may be increased up to $\beta = 1.2$ for steady-state simulations.

For viscous simulations, the same approach as above was taken to determine the stability criteria for the PCICE-FEM scheme. Morgan and Peraire [12] based the viscous stability criteria for the two-step Taylor–Galerkin FEM scheme upon the cell Peclet number. Removing the acoustic component, Morgan's viscous stability criteria gives

$$\Delta t \leqslant \frac{\alpha\beta h_\mathrm{e}^2 c_\mathrm{p}\rho}{2k + |\vec{u}|h_\mathrm{e}c_\mathrm{p}\rho}, \tag{53}$$

for $\varphi \geqslant 0.5$. This criteria works well for low to high-speed viscous flows. For very slow viscous flows (see Section 4.3), β must be reduced, on the order of $\beta = 0.5$, as the explicit diffusion terms begin to dominate.

4. Simulation results

To partially document the solution capability of the PCICE-FEM scheme, four simulations of inviscid and viscous flows ranging from nearly incompressible to highly compressible are illustrated. The first two simulations are of transient inviscid flows which demonstrate the PCICE-FEM scheme's ability to accurately propagate wave forms. The first is the classical one-dimensional shock tube problem. The second is the Sedov blast wave problem which will test the PCICE-FEM scheme's ability to maintain symmetry of an infinite strength shock wave on a non-uniform mesh. The third simulation is of low-speed viscous flow around a cylinder resulting in an oscillatory flow pattern. Finally, a high-speed, steady-state, viscous simulation is presented for a double-throated nozzle with the flow varying from Mach = 0.01–2.7.

4.1. The shock tube problem

The shock tube problem is a classic test case for the validation of compressible flow schemes and codes. It is one of the few compressible flow problems that has an analytic solution available [23] that can be

compared to numerical and experimental results. Therefore, the shock tube problem is ideally suited to test the PCICE-FEM scheme's ability to accurately propagate wave forms. The problem can be characterized by the sudden rupture of a diaphragm in a long one-dimensional tube separating two initial gas states at different pressures and densities (see the initial conditions in Fig. 1). The state after the rupture of the diaphragm ($t > 0$) consists of three propagating wave structures; a shock wave propagating downstream followed by a contact discontinuity traveling with the local fluid velocity and an expansion fan (rarefaction wave) traveling upstream.

Fig. 1 depicts the initial conditions of the shock tube problem at time $t = 0.0$ with a 10 to 1 isothermal pressure drop across the diaphragm located at $x = 40.0$ m. The two-dimensional finite element mesh for this one-dimensional problem is constructed of a 101×11 node structured grid arrangement with a 1.0 m spacing.

Figs. 2 and 3 illustrate the PCICE-FEM solution for density and pressure, respectively, at a solution time of $t = 0.08$ s. The solutions in these plots are slightly better than those obtained with our FEM-FCT code and required half the number of times steps. Total run time for the PCICE-FEM solution is 1.11 s with a time step increment of $\Delta t = 1.15 \times 10^{-3}$ s. Total run time for the equivelent FEM-FCT solution is 1.55 s with at time step increment of $\Delta t = 6.12 \times 10^{-4}$ s. Both of these simulations were timed on a 1.0 GHz AMD K7 personal computer.

The plots in Figs. 2 and 3 were created with the nodal values of the variables taken along the center line of the finite element mesh ($y = 5.0$ m). The PCICE-FEM solution obtained on this uniform mesh is symmetric about the centerline. Fig. 4 depicts the relative error between the centerline solution and the solid wall solutions located at $y = 0.0$ and $y = 10.0$ m. Only in the vicinity of the shock does the relative error approach 1.0%.

4.2. The Sedov blast wave problem

The Sedov [24] blast wave problem can be characterized as an intense point explosion in a uniform perfect gas, initially at rest, with negligible inital pressure and finite initial density. We chose the Sedov blast wave problem to demonstrate the ability of the PCICE-FEM scheme to simulate strong shock propagation and to maintain solution symmetry on non-uniform meshes. Three cylindrical blast wave simulations were performed on orthoganal triangular meshes consisting of 51×101, 101×201, and 201×401 nodes (with the same structured node arrangement shown in Fig. 1). A square domain of 1000 m sides, which results in $\Delta x = 2\Delta y$, was chosen to model one quadrant of the cylindrical blast wave. A large amount of internal

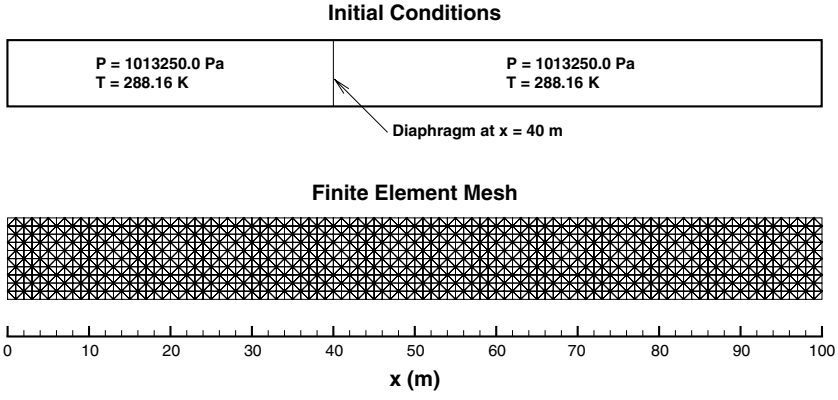

Fig. 1. Initial conditions and finite element mesh for the shock tube problem.

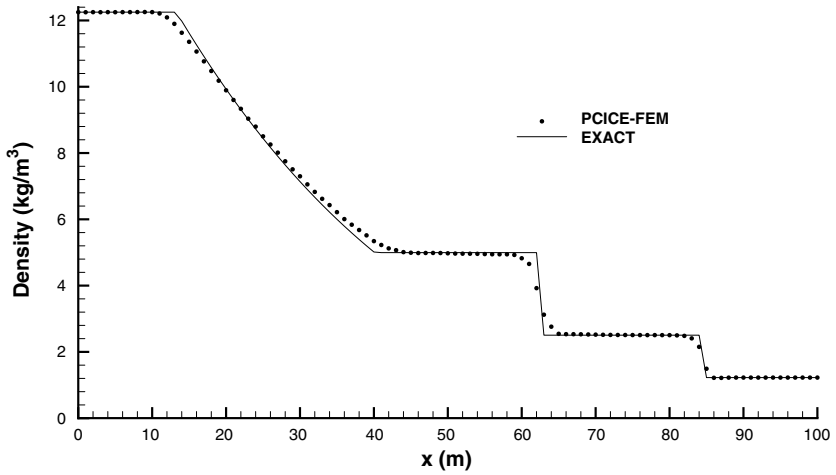

Fig. 2. PCICE-FEM shock tube solution for density at time $t = 0.08$ s.

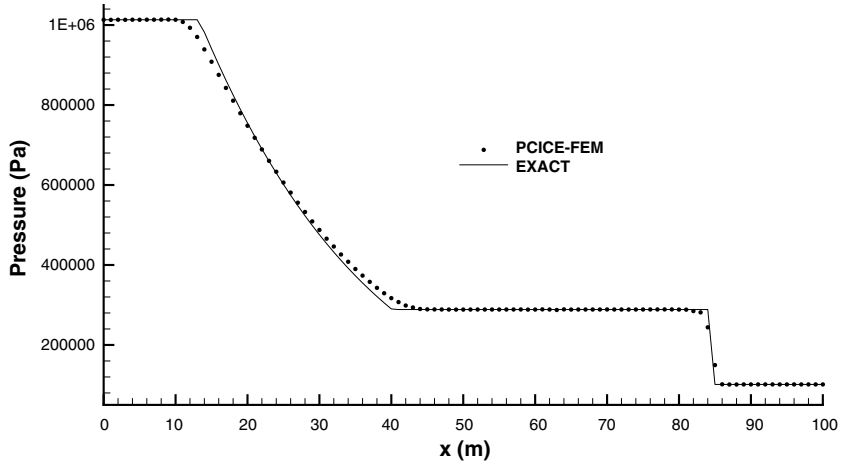

Fig. 3. PCICE-FEM shock tube solution for pressure at time $t = 0.08$ s.

energy, 6.25×10^{12} J, was instantly deposited in the first four elements defining a square adjacent to the origin ($2\Delta y$ high in the y-direction and Δx wide in the x-direction), so that the initial conditions are symmetric about the 45° line. The analytic solution for 2.5×10^{13} J deposited at the origin (total of all four quadrants) with an initial density of $\rho_0 = 1.25$ kg/m^3 results in a shock wave location of 822.3 m from the origin 0.15 s after the explosion is initiated.

Fig. 5 illustrates the blast wave solution (normalized to the initial conditions) computed on the 201×401 mesh. Peak density occurs along the y-axis where the element spacing is the smallest. Symmetry appears to be well maintained as the blast wave location along both axes is very close to the analytic location, despite the variation in mesh spacing to time step ratio.

Solution symmetry can be further scrutinized by examining the expanded plots shown in Figs. 6 and 7 of the shock front region. For $\gamma = 1.4$, the analytic solution gives the shock density to be $\rho_s = 6.0\rho_0$. Fig. 6

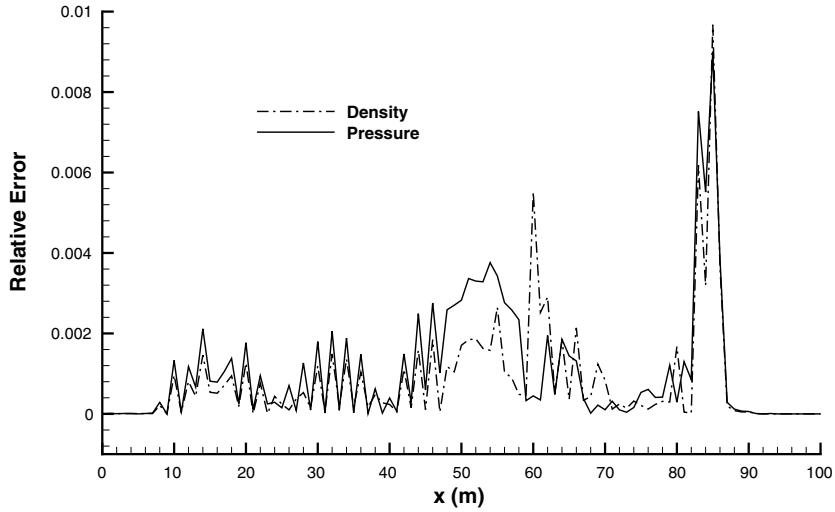

Fig. 4. Relative error between centerline and wall values of density and pressure.

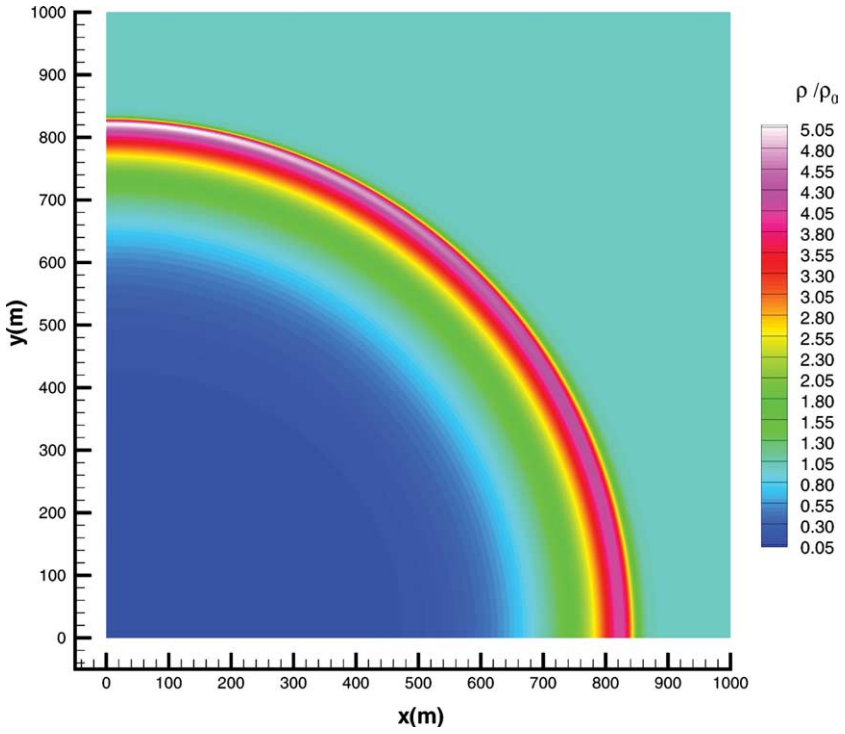

Fig. 5. Cylindrical Sedov blast wave density solution on 201×401 mesh, $t = 0.15$ s.

illustrates the comparison of the analytic density solution with the numerical density solution along the x-axis for the three meshes. With the larger element spacing along the x-axis, the numerical solution appears to lead the analytic solution by one or two elements. Fig. 7 compares the analytic density solution with the

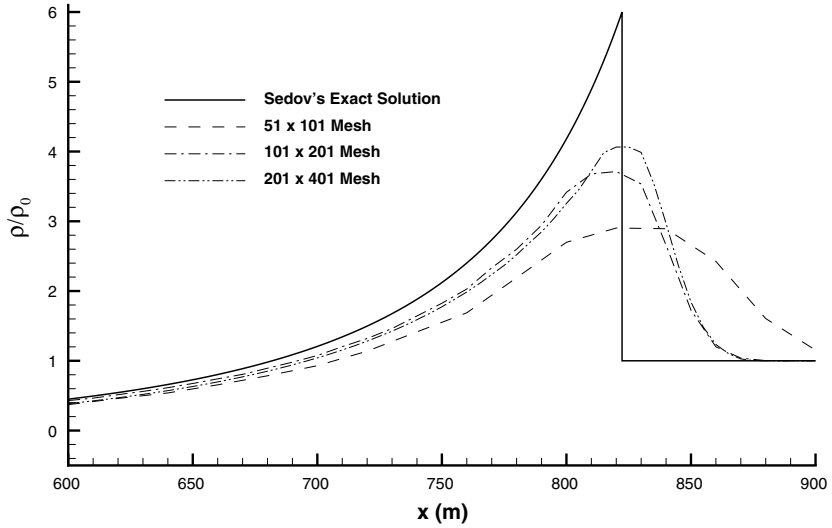

Fig. 6. Comparison of density solutions in the vicinity of the blast wave along the x-axis, $t = 0.15$ s.

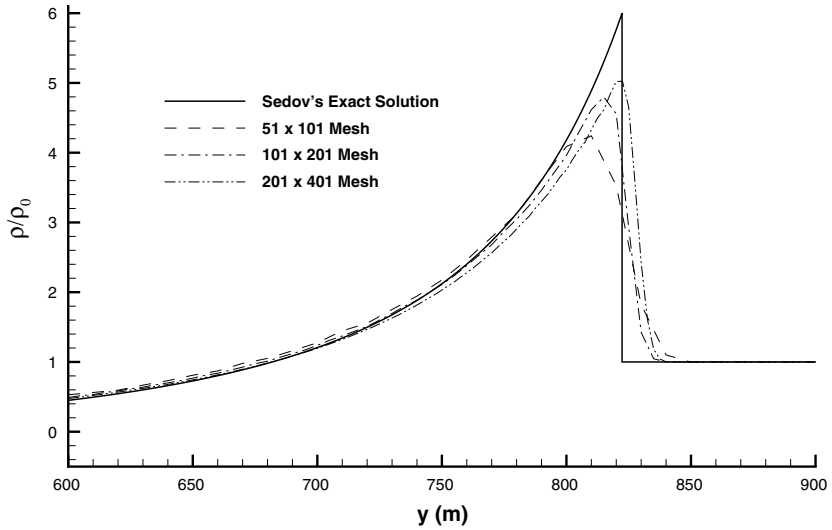

Fig. 7. Comparison of density solutions in the vicinity of the blast wave along the y-axis, $t = 0.15$ s.

numerical density solution along the y-axis. Obviously, the numerical solution compares well with the analytic solution due to the smaller mesh spacing and the local stability requirement in this region dictating the global time step size.

4.3. Low-speed viscous flow around a cylinder (Von Karman vortex street)

Low Reynolds number flow around a cylinder in a cross flow is a common benchmark problem for transient algorithms employing the incompressible Navier–Stokes equations. The problem is idealized by an infinitely long cylinder placed in free stream flow normal to the axis of the cylinder. Beyond a critical

Reynolds number of $Re > 40$ [25], the solution becomes unsteady and a periodic shedding of vortices occur, known as the von Karman vortex street. These vortices are laminar for Reynolds numbers in the approximate range of $40 < Re < 5000$.

The computational domain for the von Karman vortex street simulation is shown in Fig. 8. The inlet boundary is located at $x = -5.0$ m and the exit boundary is located at $x = 20.0$ m. The boundaries located at $y = -7.5$ and $y = 7.5$ m are prescribed free-slip solid walls. A 1.0 m diameter cylinder is located at $x = y = 0.0$ m. The finite element mesh consists of 26,068 nodes and 51,786 triangular finite elements.

The flow parameters of the von Karman vortex street simulation are defined in terms of the compressible Navier–Stokes equations. The free stream velocity is equivalent to a Mach number of $M = 0.05$. At a free stream temperature and pressure of $T_\infty = 300.0$ K and $P_\infty = 101325.0$ Pa, respectively, the free stream velocity is $V_\infty = 17.36$ m/s. For a Reynolds number of $Re = 100$, the resulting free stream dynamic viscosity is scaled to $\mu_\infty = 0.2043$ (N s)/m^2 over the entire domain. At the inlet boundary, the y-component of velocity is set to zero. The subsonic exit boundary is specified with a pressure of $P = 101325.0$ Pa. Adiabatic, no-slip boundary conditions are applied at the solid wall of the stationary cylinder.

Figs. 9–11 are the flooded contour representations of the solution to the von Karmen vortex street problem at $t = 4.0$ s for pressure, temperature, and Mach number. The periodic oscillations in the solution of this problem are clearly visible for each contoured variable. The pressure solution represented in Fig. 9 clearly shows the low-pressure center of each vortex propagating downstream from the stationary cylinder. The PCICE-FEM pressure solution slightly over-predicts the stagnation pressure at the stagnation point in front of the cylinder by approximately 19 Pa due to very slight numerical oscillations in the flow variables in this region. The temperature solution illustrated in Fig. 10 is the most dramatic representation of the flow field. The maximum variation in temperature across the domain is on the order of 0.25 K. With negligible compression, this small variation in temperature must be due to viscous heating. Note that the track of the fluid is at a higher temperature than the surrounding ambient fluid temperature of 300.0 K. As with pressure, there is a slight over-prediction of 0.011 K for the stagnation temperature.

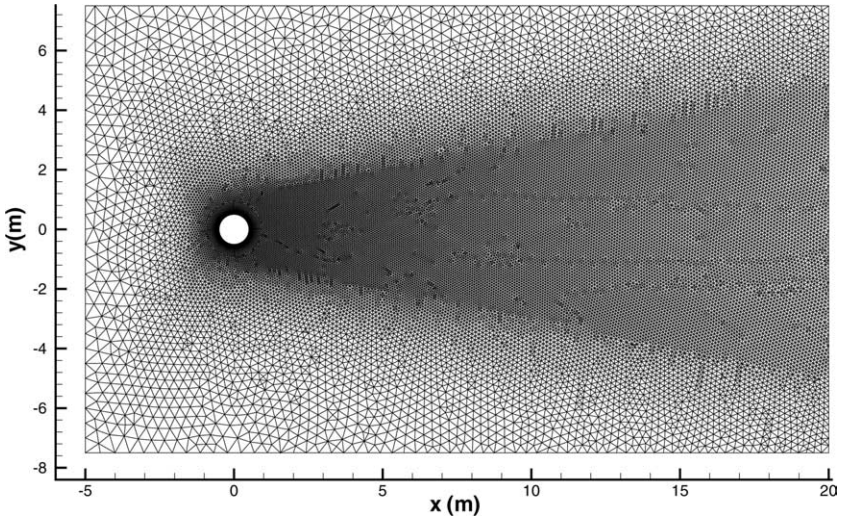

Fig. 8. Finite element mesh for the von Karman vortex street simulation.

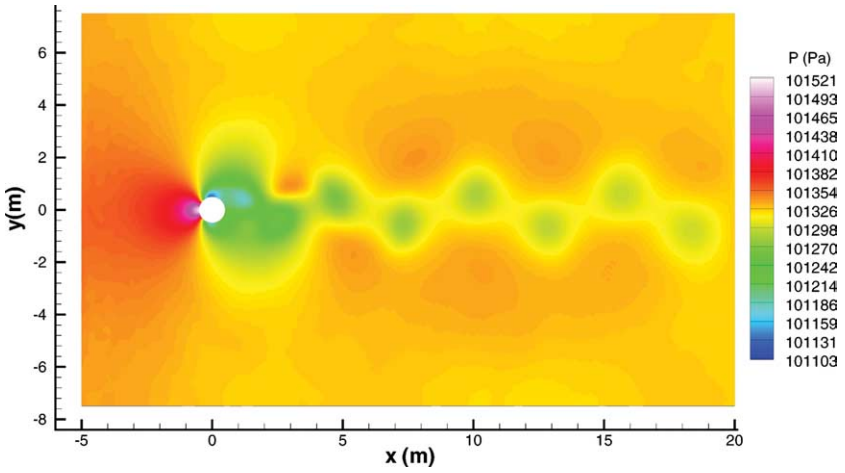

Fig. 9. Von Karman vortex street pressure solution at time $t = 4.0$ s.

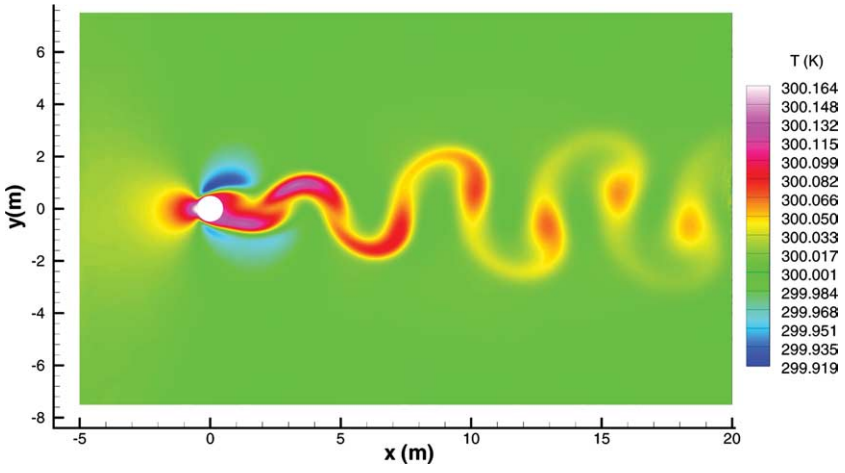

Fig. 10. Von Karman vortex street temperature solution at time $t = 4.0$ s.

4.4. Double-throated nozzle (The GAMM problem)

The viscous double-throated nozzle simulation presented in this section originated from the 1987 GAMM workshop [26]. This problem was the second of two test cases designed with the aim of generating strong viscous interaction phenomena in steady-state, laminar compressible flows inside a well-bounded domain. Supersonic flow conditions are obtained in the first converging–diverging nozzle. Then the wall is turned concave toward the second converging–diverging nozzle. It is in the middle diverging–converging section, with partly supersonic flow conditions, that compression waves, oblique shock waves, and boundary layer separations are expected to occur. After the second throat, the flow is allowed to expand rapidly in the second diverging section.

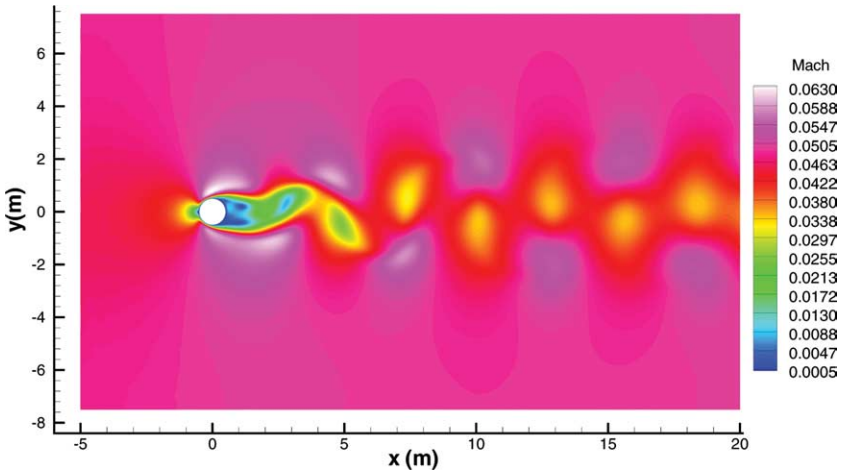

Fig. 11. Von Karman vortex street Mach number solution at time $t = 4.0$ s.

The problem geometry and finite element mesh for the double-throated nozzle problem is shown in Fig. 12. Only half of the mesh shown was used for the computation as there is a symmetry plane defined at $y = 0.0$ m. The solid wall is defined by a complex set of clamped cubic splines [26]. Dense clustering of the linear triangular finite elements near the solid wall was performed in order to resolve the boundary layer phenomena. This adapted mesh is the result of a single h-refinement [5] based upon variations in density. The inlet is located at $x = -12.0$ m and the exit is defined by the surfaces for $x > 14.0$ m.

The operating parameters for this simulation are defined by an inlet reservoir and an isothermal solid wall. Reservoir conditions, or stagnation conditions, applied at the inlet were chosen to be $P_0 = 253312.5$ Pa and $T_0 = 400.0$ K with the y-component of velocity suppressed. The solid wall is defined as no-slip and isothermal with the wall temperature set to the stagnation temperature, $T_w = T_0$. The exit boundary surfaces are supersonic, thus they are left free and nothing is specified. The Reynolds number for this problem is set to $Re = 1600$, where the Reynolds number is defined [26] as

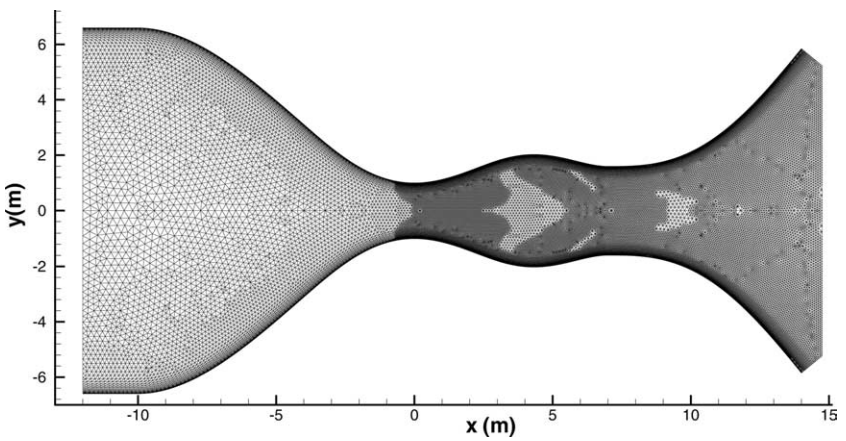

Fig. 12. Adapted finite element mesh for the GAMM nozzle simulation.

$$Re = \frac{\rho_0 a_0 L}{\mu_0}. \tag{54}$$

For this Reynolds number, L is the nozzle half-height located at the first throat, $x = 0.0$ m, and is chosen here to be $L = 1.0$ m. In Eq. (54), a_0 and ρ_0 are the stagnation sound speed and density. These parameters define a constant dynamic viscosity value of $\mu_0 = 0.5528$ (N s)/m^2. The initial conditions were designed to guarantee supersonic flow at the exit.

The PCICE-FEM solution of the double-throated nozzle simulation is depicted in Figs. 13–15 for pressure, temperature, and Mach number, respectively. The solution incorporated FCT as the high-resolution filter for shock capturing. The PCICE-FEM solution compares well with the results documented in the GAMM workshop [26]. However, there was one exception. There are two boundary layer separation/re-attachment regions, or recirculation bubbles. The first is located just downstream from the first throat. This bubble is caused by an adverse pressure gradient in the first diverging section. The second recirculation

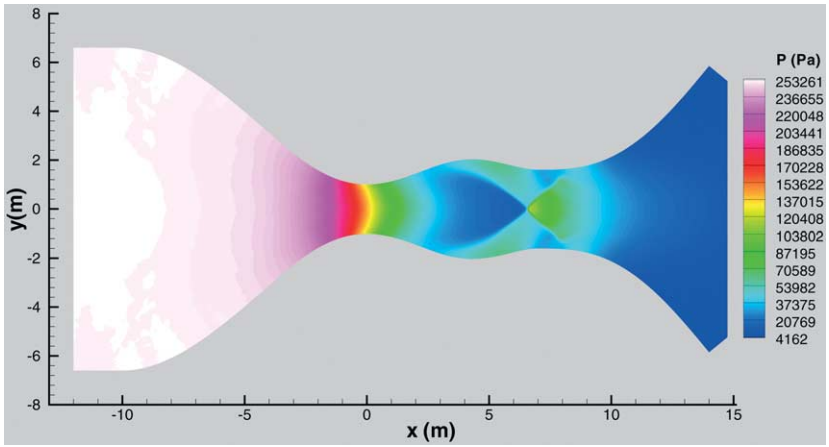

Fig. 13. PCICE-FEM pressure solution for the GAMM nozzle simulation.

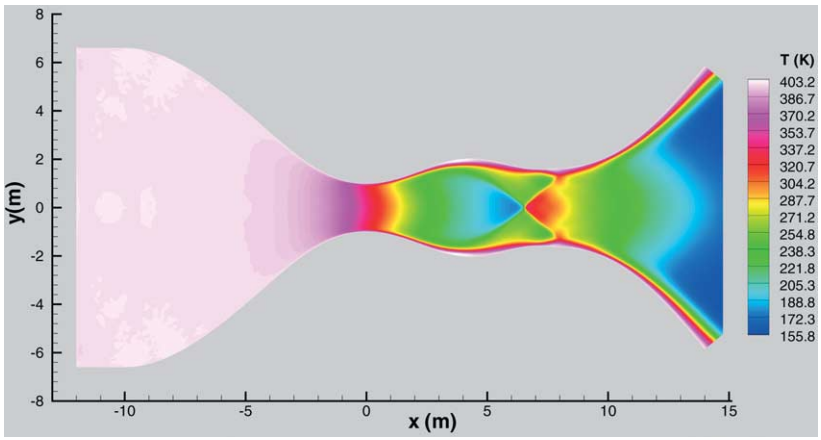

Fig. 14. PCICE-FEM temperature solution for the GAMM nozzle simulation.

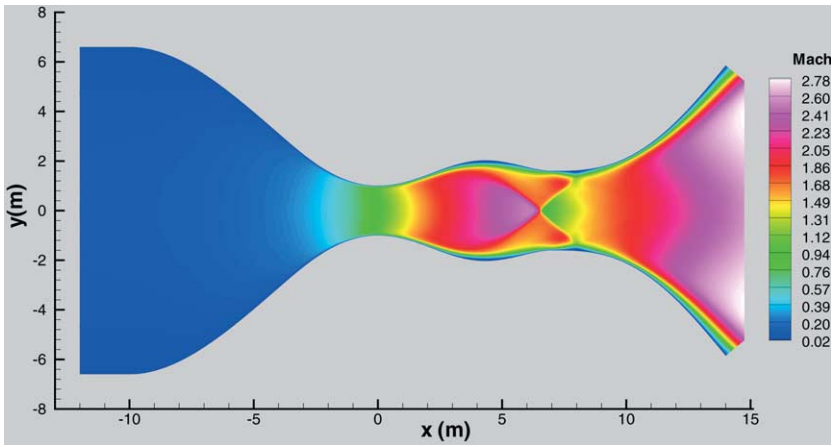

Fig. 15. PCICE-FEM Mach number solution for the GAMM nozzle simulation.

bubble appears just downstream of the second throat and is due to the interaction between the impinging oblique shock wave and the viscous boundary layer. The PCICE-FEM solution generates these recirculation bubbles somewhat farther upstream than those in the documented workshop results. The PCICE-FEM results are believed to be more accurate due to the much finer mesh employed in the recirculation regions for this simulation than those employed by the researchers participating in the GAMM workshop.

5. Conclusions

The PCICE-FEM scheme represents an advancement in mass–momentum coupled, pressure-based schemes. The conservative form of the momentum balance, mass conservation, and the total energy equations are employed as the governing hydrodynamic equations for this scheme. These governing equations are temporally discretized in a time-weighted, semi-implicit form. The PCICE-FEM scheme was developed as a predictor–corrector scheme by employing a fractional-step splitting of the semi-implicit temporal discretization of the governing equations. The semi-implicit equations in the PCICE-FEM scheme were cast as an explicit predictor phase and a semi-implicit pressure-correction phase with the elliptic pressure Poisson solution coupling the predictor–corrector phases. This predictor–corrector formulation provides the pressure Poisson equation with sufficient internal energy information to avoid iteration with the semi-implicit form of the governing equations. The ability of the PCICE-FEM scheme to accurately and efficiently simulate a wide variety of inviscid and viscous compressible flows was demonstrated. The scheme produced excellent results when simulating strong transients and maintained good symmetry on non-uniform meshes (see Sections 4.1 and 4.2). The scheme excels on low-speed viscous transient (see Section 4.3) and viscous high-speed steady-state simulations (see Section 4.4) because of the larger time step size, residual smoothing, and the new Jacobi preconditioning matrix developed for the Bi-CGSTAB solver.

Acknowledgements

The authors would like to acknowledge the US Department of Energy, Office of Environmental Management for funding the preparation of this manuscript under DOE Idaho Operations Office Contract DE-AC07-99ID13727.

References

[1] F.H. Harlow, A.A. Amsden, Numerical calculation of almost incompressible flow, J. Comput. Phys. 3 (1968) 80.
[2] F.H. Harlow, A.A. Amsden, A numerical fluid dynamics calculation for all flow speeds, J. Comput. Phys. 8 (1971) 197.
[3] R.C. Martineau, R.A. Berry, An efficient, semi-implicit pressure-based scheme employing a high-resolution finite element method for simulating transient and steady, inviscid and viscous, compressible flows on unstructured grids, INEEL Report No. INEEL/EXT-03-00490, 2003.
[4] R. Löhner, K. Morgan, O.C. Zienkiewicz, An adaptive finite element procedure for compressible high speed flows, Comput. Meth. Appl. Mech. Engrg. 51 (1985) 441.
[5] R. Löhner, K. Morgan, J. Peraire, M. Vahdati, Finite element flux-corrected transport (FEM-FCT) for the Euler and Navier–Stokes equations, Int. J. Numer. Meth. Fluids 7 (1987) 1093.
[6] R. Löhner, K. Morgan, M. Vahdati, J.P. Boris, D.L. Book, FEM-FCT: combining unstructured grids with high resolution, Commun. Appl. Numer. Meth. 4 (1988) 717.
[7] H.A. van der Vorst, BI-CGSTAB: a fast and smoothly converging variant of BI-CG for the solution of non-symmetric linear systems, SIAM J. Sci. Statist. Comput. 13 (2) (1992) 631.
[8] F.H. Harlow, J.E. Welch, Numerical calculation of time-dependent viscous incompressible flow of fluids with free surface, Phys. Fluids 8 (1965) 2182.
[9] F.H. Harlow, J.E. Welch, J.P. Shannon, B.J. Daly, The MAC Method, Los Alamos Scientific Laboratory, LA-3425, 1965.
[10] A.J. Chorin, A numerical method for solving incompressible viscous problems, J. Comput. Phys. 2 (1967) 12.
[11] C.K. Westbrook, A Generalized ICE method for chemically reactive flows in combustion systems, J. Comput. Phys. 28 (1978) 67.
[12] K. Morgan, J. Peraire, Finite element methods for compressible flows, von karman institute for fluid dynamics, Lecture Series 1987-04, March 2-6, 1987.
[13] J. Donea, A Taylor–Galerkin method for convective transport problems, Int. J. Numer. Meth. Engrg. 20 (1984) 101.
[14] A. Jameson, T.J. Baker, N.P. Weatherhill, Calculation of inviscid transonic flow over a complete aircraft, AIAA-86-0103, 1986.
[15] R.C. Swanson, E. Turkel, On central-difference and upwind schemes, J. Comput. Phys. 101 (1992) 297.
[16] J. Peraire, J. Peiro, L. Formaggia, K. Morgan, O.C. Zienkiewicz, Finite element Euler computations in three dimensions, Int. J. Numer. Meth. Engrg. 26 (1988) 2135.
[17] A. Jameson, W. Schmidt, E. Turkel, Numerical solution of the Euler equations by finite volume methods using Runge–Kutta time-stepping schemes, AIAA-81-1259, 1981.
[18] R. Löhner, Applied CFD Techniques, John Wiley & Sons, London, 2001, p. 172.
[19] G.E. Georghiou, R. Morrow, A.C. Metaxas, An Improved finite-element flux-corrected transport algorithm, J. Comput. Phys. 148 (1999) 605.
[20] P.M. Gresho, R.L. Sani, On pressure boundary conditions for the incompressible Navier–Stokes equations, in: Finite Elements in Fluids, vol. 7, John Wiley & Sons, New York, 1987.
[21] P.M. Gresho, R.L. Sani, Incompressible Flow and the Finite Element Method, John Wiley & Sons, New York, 1999.
[22] A.E.P. Veldman, Missing boundary conditions? Discretize first, substitute next, and combine later, SIAM J. Sci. Statist. Comput. 11 (1) (1990) 82.
[23] C. Hirsch, Computational methods for inviscid and viscous flows, in: Numerical Computation of Internal and External Flows, vol. 2, John Wiley & Sons, New York, 1990.
[24] L.I. Sedov, Similarity and Dimensional Methods in Mechanics, Academic Press, New York, 1959.
[25] F.M. White, Viscous Fluid Flow, second ed., McGraw-Hill InclocationNew York, 1991.
[26] M.O Bristeau, R. Glowinski, J. Periaux, H. Viviand, Numerical Simulation of Compressible Navier–Stokes Flows, GAMM-Workshop, Friedr. Vieweg & Sohn, London, 1987.